Particle re-acceleration in 3D current sheets in the heliosphere and their diagnostics from observations

V.V. Zharkova[1], Q. Xia[1,2], O.V. Khabarova[3], O.Malandraki[4] https://iopscience.iop.org/article/10.3847/2041-8213/ab8cb8/pdf

[1]University of Northumbria, UK; [2]Culham Space Centre, UK; [3]IZMIRAN, Russia; [4]Observatory of Athens, Greece

Summary

- This research aims to explore variations of electron pitch-angle distribution (PAD) during spacecraft cross reconnecting current sheets (RCSs) with magnetic islands. The results can benchmark the sampled characteristic features with realistic PADs derived from in-situ observations.
- Particle motion is simulated in 2.5D Harris-type RCSs using particle-in-cell (PIC) method considering the plasma feedback to electromagnetic fields. We evaluate particle energy gains and PADs in different locations and under the different directions of passing the current sheet by a virtual spacecraft. The RCS parameters are comparable to heliosphere and solar wind conditions.
- The energy gains and the PADs of particles would change depending on the specific topology of magnetic fields.
- Besides, the observed PADs also depend on the crossing paths of the spacecraft. When the guiding field is weak, the bi-directional electron beams (strahls) are mainly present inside the islands and located closely above/below the X-nullpoints in the inflow regions. The magnetic field relaxation near X-nullpoint converts the PADs towards 90◦.
- As the guiding field becomes larger, the regions with bi-directional strahls are compressed towards small areas in the exhausts of RCSs. Mono-directional strahls are quasi-parallel to the magnetic field lines near the X-nullpoint due to the dominant Fermi-type acceleration.
- Meanwhile, the high-energy electrons confined inside magnetic islands create PADs about 90◦.

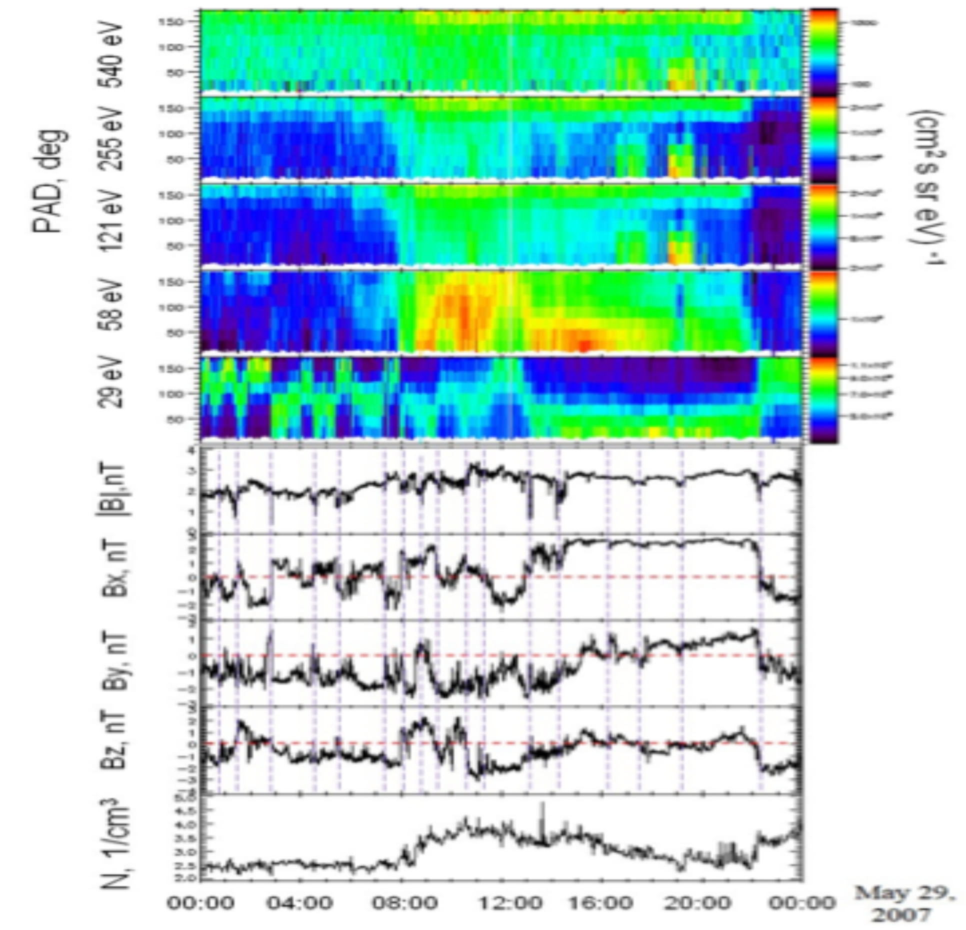

Fig. 2. The electron PADs of different energies, the IMF, and the density in the region filled with MIs of variable size as observed by the WIND spacecraft on 2007 May 29. From top to bottom: PADs of electrons measured with ~24 s resolution in the following channels: Channel 3 (often ~540 eV); Channel 5 (often ~255 eV); Channel 7 (often ~121 eV); Channel 9 (often ~58 eV); Channel 11 (often ~29 eV); the IMF strength; the three IMF components in the GSE system; and the solar wind density. Crossings of CSs separating MIs are shown by vertical dashed purple lines.

2. Observations

Fig. 1 shows the corresponding observations of the key solar wind parameters at ~1 AU. The stream interaction region (SIR) was detected by the L1 spacecraft (Figure 1a) practically simultaneously with STEREO A (Figure 1b), and then the plasma reached STEREO B (Figure 1b). This feature indicates a strong twist of the SIR front with respect to the Parker spiral, since normally it is observed by STEREO B first (Gomez-Herrero et al. 2011). The MI-containing region observed on 2007 May 28-31was characterized by very similar profiles of the key parameters detected by all the spacecraft with an unusually minimal time-shift. Therefore, plasma samples under current study from the center of the region (May 29, 2007) correspond to the same as analyzed in Khabarova et al. (2016).

MIs can be seen in Figure 2 as intense anticorrelated variations in the IMF components, not stochastic as usually seen in simple turbulent regions, but appearing as humps of approximately an hour in length (more about signatures of MIs can be found in Khabarova et al. 2015, 2016; Khabarova & Zank, 2017). The vertical dashed lines indicate borders of MIs, and each border represents a current sheet. Analyzing the lower (black and white) panels of Figure 2 with IMF and density parameters, one can note that the MIs with the largest IMF strength and the slightly elevated density are observed from ~8 UT. Such conditions lead to intensification of magnetic reconnection in the region. The largest MIs are observed from 13 UT to 22 UT. Overall, the IMF patterns show the presence of smaller-scale dynamic MIs in the left part of Figure 2, the main reconnecting relatively large MIs in the middle, and the larger but more stable MIs in the right part.

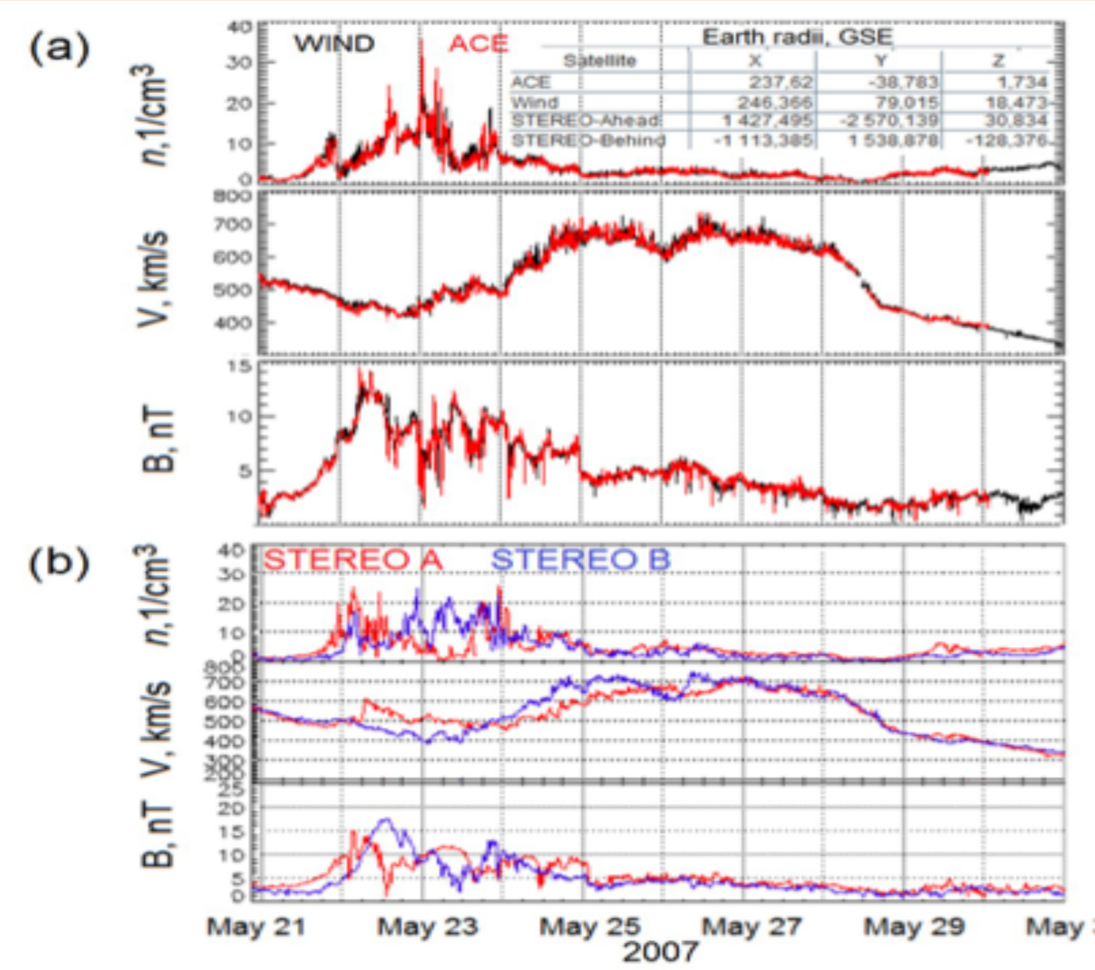

Fig. 1. Three panels in (a) and (b) from top to bottom are the solar wind density, the solar wind speed, and the IMF strength obtained from the L1 (ACE and WIND) spacecraft (a) and the STEREO A and STEREO B spacecrafts.

It is evident that electrons of different energies behave differently.

- Electrons in the lowest energy 11 channel closely follow the magnetic topology of smallest and dynamical MIs (see the up-and-down variations occurring in accordance with most intense variations in the IMF).
- It is known that usually PAD patterns vary rather slowly from channel direction of the electron motion shows a clear anticorrelation of variations of pitch angles with respect to the patterns seen in higher-energy channels 7 and 5.
- Furthermore, the most intense flux follows the position of the most intensely reconnecting MIs in the middle of Figure 2 (compare the bird-like red PAD pattern and large-scale variations in Bx).
- The channel 5 PAD indicates uninterrupted/smooth strahl flowing in the sunward direction (the color stripe at the top of the PAD in the left part of the panel) until the approach to the region of the strongest and largest reconnecting MIs in the middle of Figure 2. From ~8 UT, the intense dispersionless vertical feature is seen in the 5-9 channel PADs (green vertical region), and in the area of large and rather undisturbed MIs there are features of bi-directionality seen in the higher-energy 3-7 channel PADs. The PAD for channel 5 looks similar to channel 7.
- The PAD of suprathermal electrons in channel 3 shows signatures of counter-streaming strahls (red and yellow stripes at 0□ and 180□) in the background of the intense dispersionless halo (green).

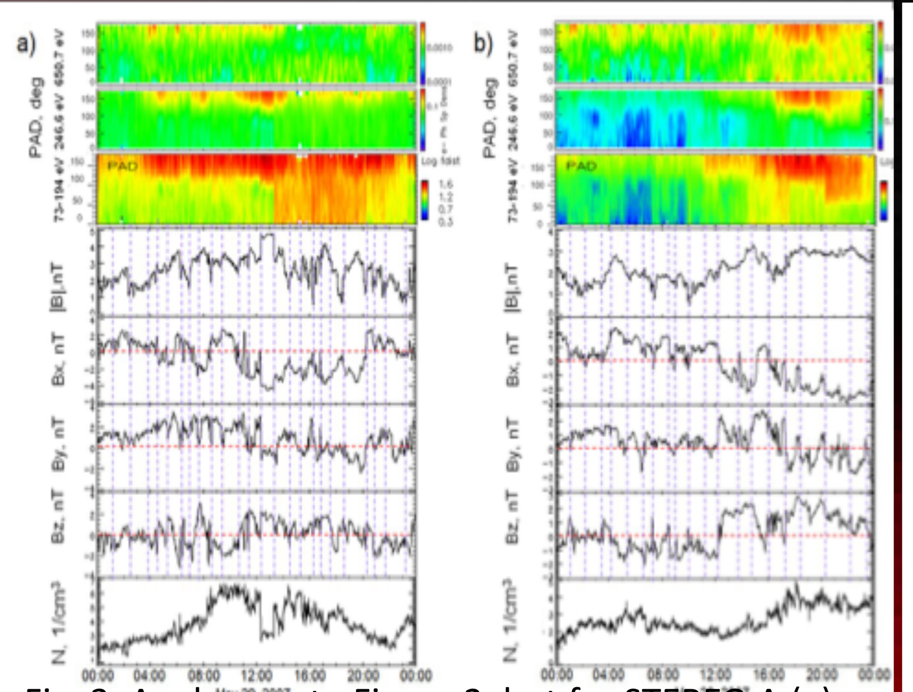

Fig. 3. Analogous to Figure 2, but for STEREO A (a) and STEREO B (b). Upper PAD panels are for the 650.7, 246.6, and 73-194 eV energy channels.

The behavior of suprathermal electrons in both the lower PAD 73-194 eV panels in Figures 3(a) (STEREO A) and (b) (STEREO B) generally reflects the PAD features seen in the 58-121 eV WIND energy channels in Figure 2 with a corresponding short time-shift. STEREO PAD patterns in the 246.6 eV channel (the middle PAD panels of Figure 3) are consistent with WIND 255 eV PAD in Figure 2 in which the formation of sunward-directed strahl stripe can be observed. The highest-energy 650.7 eV STEREO PAD in Figure 3 is completely different from the other PADs.

It shows signatures of intermittent bi- directionality, following the location of MIs and CSs, very similar to the lower-energy PADs of WIND (Figure 2), especially in the region with the largest MIs and the local density increase (see Figure 3b).

3. Simulations

In order to understand the PAD features discussed above and to test the idea about the existence of locally borne suprathermal electrons, we show key results of simulations of properties of electrons accelerated in typical RCS and MI configurations, considering the ambient plasma feedback to the presence of accelerated particles discussed in Xia and Zharkova (2020).

We trace particles in the vicinity of a 3D current sheet with a half-width of one gyroradius (d=1.0pi along X) extended along Z. B is the static magnetic field induced by magnetic reconnection. The reconnection electric field Ey accelerating particles is perpendicular to the reconnection plane.

- Particles from the ambient neutral plasma are dragged into the reconnection region from both sides by the magnetic diffusion process, leaving the RCS only after those gain the critical energy required to break from the magnetic field topology shown in Figure 4a (see details in Zharkova & Gordovskyy 2005; Xia & Zharkova 2018, 2020). After that, particles with opposite charges (electrons versus protons/ions) are ejected into the opposite semiplanes.
- Particles of the same charge form two distinct groups ('transit' and 'bounced') with very different energies and trajectories (Figure 4a). The maximal energy reached by each population depends on By. (Siversky & Zharkova, 2009; Xia & Zharkova, 2018).
- If By/B0 varies from 0 to 1, bounced electrons (lower-energy electrons, bottom panels in Figure 4b) can be accelerated to energies with the upper threshold from 20eV to 500eV, respectively, while transit electrons gain energies approaching hundreds of keV (higher-energy electrons, upper panels in Figure 4b).

Figure 4b shows that the both populations behave very differently, forming different PAD patterns, which are sensitive to By and d. PADs of electrons accelerated in CSs without the guide field By/B0=0 are quite symmetric with respect to the midplane, but when By increases, asymmetry increases respectively.

If dynamical MIs occur in an RCS, even more complex PADs compared to those shown in Figure 4b can be observed. Xia and Zharkova (2020) modeled particle acceleration in squashed (contracting) and coalescent (merging) MIs formed in RCSs.

- The model of a current sheet with multiple X- and O-nullpoints (MIs) is adopted from Kliem (1994) and described in detail by Xia and Zharkova (2020). Here we show an example of a PAD observed by a virtual spacecraft crossing the system of two merging MIs and CSs surrounding them (Figure 5). A complex PAD with a clear signature of bi-directionality is observed within the MIs in the higher-energy channel (the same feature is seen in squashed MIs in a narrower area centered in the middle of an MI – not shown). At the same time, at edges of dynamical MIs, PAD patterns may vary from dispersionless to completely defocused. Lower-energy electrons do not leave MIs showing the most intense PAD profiles at their edges.
- Lower- and higher-energy electrons produce differently appearing PADs, which suggests that such a difference observed in higher- and lower- energy PAD channels is

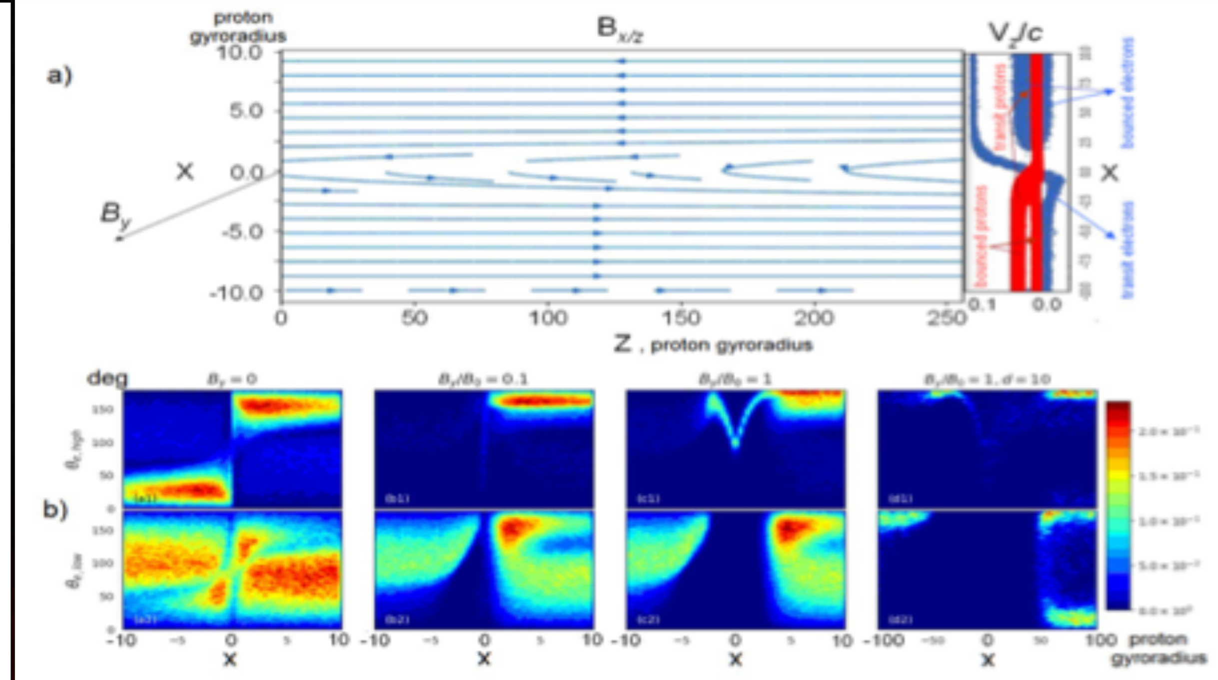

Fig. 4. Modeling of acceleration of solar wind electrons to suprathermal energies at the 3D RCS. a) Topology of magnetic field lines in the vicinity of the single X-nullpoint of the RCS (on the left), and example of 2.5D particle-in-cell simulations (3D by velocity V and 2D by coordinate) of particle trajectories for the strong guide field, By/B0 = 1 (on the right). Bounced particles form clouds at the injection side with respect to the midplane, but more energetic transit particles are ejected into the opposite semiplane. b) PADs for electrons with lower energy (bottom row) and higher energy (top row) for the guide field By of different strength: By/B0 = 0 (first column, weak guide field), 0.1 (second column), and 1.0 (third column, strong guide field). RCS width d=1.0 pi (thin RCS) in the three columns. B0 = 10-9T. The fourth column is given for comparison under condition of thicker RCS and strong guide field (By/B0 = 1, d=10 pi).

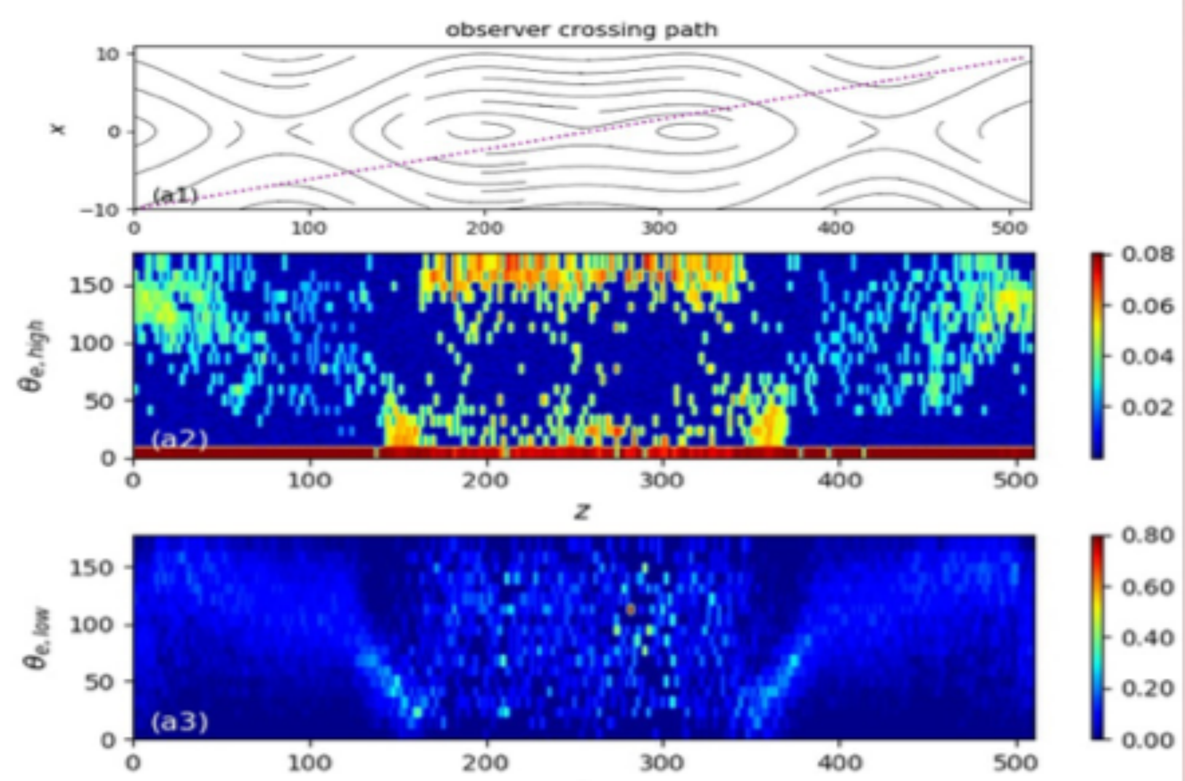

Fig. 5. PADs observed when a hypothetical spacecraft crosses two coalescent MIs. The top plot presents the magnetic field topology (black lines) and the paths of a spacecraft (purple line). Middle and bottom color plots present the PADs of higher (middle) and lower (bottom) energy electrons accelerated in the system of the islands and CSs. Parameters of the islands employed are B0 = 10-9T, E0 = 0.100m V/m, By/B0 =0.1, d = 2□i. k=L/d= 0.0325. L is the half length of the island, d is the current sheet half-thickness. Both counterstreaming strahls and dropouts may be observed in such a configuration.

4. Interpretation of observations

The electrons in the upper left PAD of Figure 4b are ejected mainly along 0◦-180◦, and the RCS midplane is clearly visible as a vertical stripe. This PAD pattern is often observed in the solar wind (see Figure 2 and Figure 3) but has always been interpreted in terms of crossing of the HCS or a similar current sheet connected to the solar source. This study shows that such a pattern just reflects a crossing of a single thin current sheet reconnecting in a weak guiding field.

- A bird-like pattern seen especially clearly in the middle of the right panel of Figure 3 and in Channel 9 of Figure 2 indicates a crossing of the CS reconnecting in a strong guide field. According to Figure 4b, it is not expected to be seen in lower-energy channels.

Figure 4b and Figure 5 suggest that an intense unidirectional PAD stripe is formed in the areas with bigger MIs (Figure 2 and Figure 3) because electrons can be accelerated to higher energies in bigger MIs, propagating much further from the initial acceleration sites (X- nullpoints or MI pools) and gradually becoming strahls that mix with solar-origin strahls and contribute to the total PAD picture in the middle- and higher-energy channels.

- Counterstreaming electrons appear naturally in the lower-energy channel of Figure 4b when the guide field is rather strong, and a huge dropout encompassing the midplane is seen in the three bottom panels (lower energy electrons) and the top right panel (higher energy electrons, strong By, and the wide RCS).

Finding this important PAD feature easily solves the mystery of the observation of numerous narrow dropouts associated with CSs in the solar wind.

Figure 5 also shows a clear signature of bi-directionality of higher-energy strahl electrons trapped and reaccelerated in dynamical MIs, while lower-energy electron paths are less structured. Wide dropouts are seen mainly in Figure 5 in the area free of merging MIs.

References. Zharkova and Gordovskyy, 2004, ApJ, 604, 884;2005, SSRv, 121, 165; Siversky and Zharkova, 2009, JPP, 75, 619; Zharkova and Khabarova, 2012, ApJ, 752, 35; 2015, Ann. Gophys., 33, 457; Khabarova et al, 2015, JPCS, 642, 012033; Khabarova, Zharkova, Xia, Malandraki, 2020, ApJL, 894, L12.